Journal of Molecular Structure 1157 (2018) 486–491

Contents lists available at ScienceDirect

Journal of Molecular Structure

journal homepage: http://www.elsevier.com/locate/molstruc

Terahertz time-domain spectroscopy of L-histidine hydrochloride monohydrate

Siqi Zong [a, b], GuanHua Ren [b, c], Shaoping Li [a, *], Bo Zhang [a, b], Jianbing Zhang [b], Wenpeng Qi [b], Jiaguang Han [c], Hongwei Zhao [b, **]

[a] School of Chemical Engineering, East China University of Science and Technology, Shanghai 200237, China
[b] Division of Interfacial Water and Key Laboratory of Interfacial Physics and Technology, Shanghai Institute of Applied Physics, Chinese Academy of Sciences, Shanghai 201800, China
[c] Center for Terahertz Waves and College of Precision Instrument and Optoelectronics Engineering, and Key Laboratory of Optoelectronics Information and Technology, Ministry of Education, Tianjin University, Tianjin 300072, China

ARTICLE INFO

Article history:
Received 20 September 2017
Received in revised form
29 November 2017
Accepted 26 December 2017
Available online 28 December 2017

Keywords:
L-histidine hydrochloride monohydrate
Low-frequency vibration
Terahertz absorption spectrum
Temperature effect

ABSTRACT

The low-frequency absorption spectrum of L-histidine hydrochloride monohydrate (LHHM) over 0.5–4.0 THz was measured by terahertz time-domain spectroscopy (THz-TDS). The comparison between the THz absorption spectra of LHHM and L-histidine (LHis) was made. The two distinctive THz spectra of LHHM and LHis indicate that THz spectroscopy is sensitive to different specimens. The low-temperature THz spectral features of LHHM presented the blue-shift and splitting as the temperature decreased. Solid-state density functional theory (DFT) calculation of the vibrational modes of LHHM was performed for better understanding the THz characteristic spectrum, and the validity of the calculation modes was confirmed by comparing with the experimental observations. Powder X-ray diffraction (PXRD) was also carried out to check the structures of LHHM and LHis.

1. Introduction

L-histidine (L-his, or LHis) is an indispensable amino acid with an imidazole ring, which constitutes the active center of many enzymes and function protein and controls the transmission of metal elements in biological bases [1]. As one of the twenty proteinogenic amino acids, L-his has been characterized and investigated by many spectroscopic techniques for its versatile functions in proteins and enzymes [2–4]. Along with L-his, its analogs have attracted attention since L-his tetrafluoroborate was found as a new promising nonlinear optical (NLO) material for frequency conversion by Marcy et al. [5]. Recently, other semiorganic NLO crystals of L-his salts which combine the advantages of the organic amino acid with that of the inorganic salt have been studied intensively [6–8]. L-histidine hydrochloride monohydrate (LHHM) as a novel semiorganic NLO material has also been characterized by vibrational spectroscopy, which can provide information about the molecular composition, structure and interactions within a sample [9]. Anandan et al. [10] grew single crystal LHHM with slow evaporation solution growth technique and investigated the absorption characterize of functional groups with Fourier transform infrared (FTIR) and FT-Raman spectroscopy. Ahmed et al. [11] recorded FTIR spectrum of single crystal LHHM in the range of 400–4000 cm^{-1}, and calculated the theoretical vibrational property using the density function theory (DFT) method to obtain reliable assignments of the experimental bands. Faria et al. [12] studied the temperature effect of LHHM with Raman spectroscopy, and suggested that the sample may have undergone phase transformation at low temperature 110–140 K.

Comparing with mid-infrared spectroscopy, terahertz time-domain spectroscopy (THz-TDS) is highly sensitive to the hydrogen bond, lattice vibration and water of crystallization [13,14]. Most crystalline solids contain distinct and characteristic lattice vibrations within this energy range, which allows THz spectroscopy a powerful analytical tool for probing the intermolecular interactions of molecular crystals [15]. The novel spectroscopic technique is widely used to investigate various amino acids in the lower end of the far-infrared region [16–18]. For instance, True et al. [16] characterized the absorption spectra of the commercial polycrystalline L-, D-his enantiomers and the DL-his racemate and

* Corresponding author.
** Corresponding author.
E-mail addresses: spli@ecust.edu.cn (S. Li), zhaohongwei@sinap.ac.cn (H. Zhao).

https://doi.org/10.1016/j.molstruc.2017.12.088
0022-2860/

observed that each sample has a unique THz fingerprint, which demonstrates the strength of THz spectroscopy in the area of polymorphism. Rungsawang et al. [17] observed different THz absorption spectra of single crystal L-his and the powder one. They assigned the absorption peak at 57 cm^{-1} of the crystal L-his as the hydrogen-bond contribution, and also observed a blue-shift when the network shrinks at low temperature.

In this work, we studied the properties of low-frequency vibrations, intra- and intermolecular interactions of LHHM with THz spectroscopy. As an essential amino acid, the THz absorption spectrum of LHis was also measured for comparing with its hydrochloride. The temperature effect on the THz spectrum of LHHM was discussed in the range of -190–20 °C. The frequencies of vibrational modes of LHHM were calculated using DFT method. The structures of LHHM and LHis were verified by powder X-ray diffraction (PXRD) examination.

2. Materials and methods

2.1. Materials

LHHM and LHis were obtained from J&K Co. Ltd. (≥99.0%). Cyclic olefin copolymer (COC) powder (particle size 50–100 μm) was purchased from Terahertz Photonic Co. Ltd. COC has been confirmed to be highly suitable for THz spectroscopy applications due to its negligible dispersion of refractive index and negligible absorption in the THz region [19]. The chemicals were used without further purification.

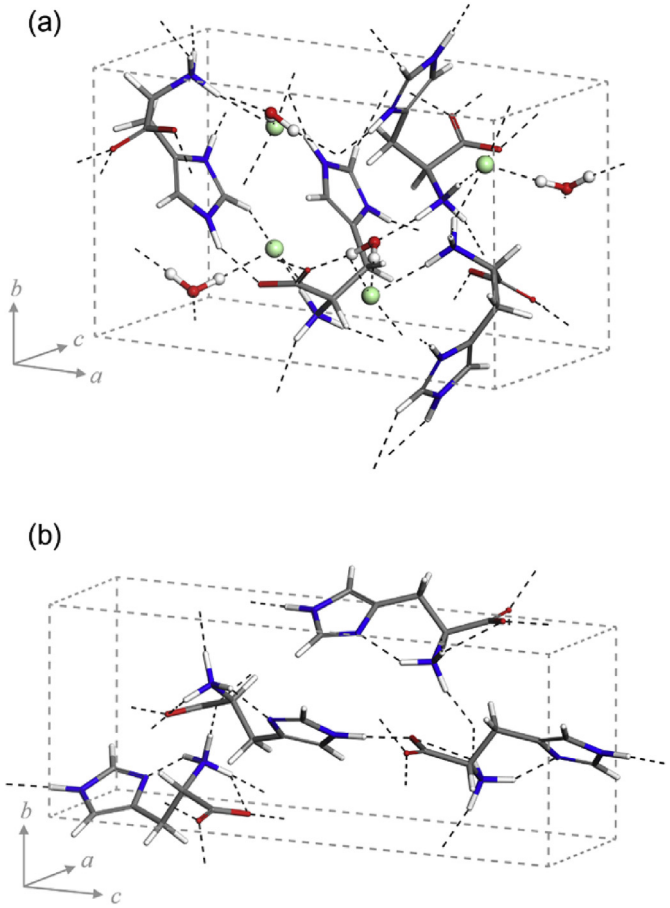

Fig. 1. The crystal structure of (a) LHHM and (b) LHis.

2.2. Sample preparation

LHHM and LHis were separately mixed with COC powder in a mass ratio of 1:10 and then pressed into tablets under a pressure of 2.0 MPa. The tablets have a diameter of 13 mm and a thickness of around 1.2 mm.

2.3. THz time-domain spectroscopy (THz-TDS)

THz spectra of LHHM and LHis were measured using a TAS7400TS THz-TDS system (Advantest Corporation, Japan. Wavelength is 1560 nm, pulse width is 300 fs and frequency resolution is 1.9 GHz). The effective spectrum band is 0.5–4.0 THz. The sample was placed into the THz system which was purged with dry air to keep the relative humidity under 1%. Each spectrum was average of three measurements with the drying air as reference. Each measurement includes 512 scan numbers.

2.4. Temperature controller

The LHHM pellet was fixed into a liquid nitrogen flowed cryostat celled with high-density polyethylene windows (Variable temperature cell holder, Specac Ltd. U.K.). A series of THz spectra of LHHM was recorded in the temperature range of -190–20 °C.

2.5. Powder X-ray diffraction (PXRD)

PXRD patterns of LHHM and LHis were recorded using the X'Pert Pro MPD (Cu source, 40 kV voltage, 40 mA filament emission). The data were collected with a scan ranging from 10° to 90° (2θ).

3. Quantum chemical calculation

The measured PXRD spectra of power LHHM and LHis match well with the previous data published in the open database Cambridge Crystallographic Data Centre (CCDC) (see Supplementary Materials Fig.S1). Therefore, our calculations were performed on their lattice parameters. Both LHHM and LHis are suggested to be orthorhombic in structure with space group $P2_12_12_1$ (Z = 4) but have differences in crystal symmetry and cell parameters. Fig. 1 shows the crystal structures of LHHM and LHis, and the corresponding lattice parameters are (a) $a = 15.36$ Å, $b = 8.92$ Å, $c = 6.88$ Å, α, β, $\gamma = 90°$ [20], and (b) $a = 5.175$ Å, $b = 7.315$ Å, $c = 18.75$ Å, α, β, $\gamma = 90°$ [21], respectively.

The geometry optimization and energy calculations were performed based on the solid-state DFT using the Cambridge Sequential Total Energy Package (CASTEP) program [22] as a part of Materials Studio package from Accelrys. The simulation of LHHM and LHis were performed based on the lattice parameters [20,21]. The results were obtained for the crystalline state within the generalized gradient approximation (GGA) at Perdew-Burke-Ernzerhof (PBE) correlation functional [23], using Grimme's dispersion-corrected method for DFT-D correction [24] and norm-conserving pseudopotential as implemented in CASTEP. The quality of energy calculation was ultra-fine. The plane-wave cutoff energy was 830 eV. For LHHM and LHis, brillouin zone sampling of electronic states were performed on $1 \times 2 \times 2$ and $3 \times 2 \times 1$ Monkhorst-Pack grid, the total energy was converged to 5.0×10^{-7} eV/atom, and the maximum forces between atoms were less than 0.01 eV/Å. The grids for fast Fourier transform were $150 \times 90 \times 72$ and $50 \times 72 \times 180$, respectively. Vibration modes of LHHM were calculated using vibrational analysis tool.

4. Result and discussion

4.1. THz absorption spectra of LHHM and LHis

Fig. 2 shows the THz absorption spectra of LHHM and LHis in the range of 0.5–4.0 THz at room temperature, and the spectra are offset vertically for clarity. LHis has six obvious peaks at 1.41, 2.09, 2.47, 2.80, 3.37 and 3.97 THz, and three relatively weaker peaks at 0.77, 1.73 and 2.99 THz. LHHM shows four obvious peaks at 2.22, 2.37, 2.90, 3.20 THz, and two less pronounced bands at 0.89 and 1.62 THz, respectively. Comparing with the structure of LHis molecule, apart from the different composition of the chloride ion (Cl^-) and water molecule, the amino acid part of the LHHM molecule is with a zwitterionic backbone and a protonated side chain [25]. And we compared the THz spectra of LHis with previous studies and listed in Table 1. It is obvious that our experimental data are partly in coherence with the observation in Ref. [17] under 3.0 THz, and basically consistent with the data obtained by reading figure in Ref. [16]. The observation of two distinctive spectra of LHHM and LHis indicates that THz spectroscopy is sensitive to structure and composition. Therefore, the characteristic THz fingerprints can be used in detection and identification applications.

4.2. Temperature effect on LHHM

The THz absorption spectra of LHHM in the temperature range of -190–20 °C are shown in Fig. 3. Forty spectra were measured, for clarity, only spectral data in the 0.5–3.5 THz range are shown. Fig. 4 exhibits the temperature effect on the absorption spectra of LHHM, spectra are vertically offset and the dashed lines are guides to the eye. Corresponding to the spectrum at 20 °C, LHHM also shows six peaks at 0.92, 1.68, 2.21, 2.39, 2.99, 3.21 THz; besides, an additional mode at 1.56 THz emerged at −190 °C. The emergence of additional mode at low-temperature can be observed more clearly in Fig. 4, which can be described as two peaks split from a broad one as well. Meanwhile, these spectra in Fig. 4 suffer different degrees of blue-shift and become distinct as temperature decreases. The observed shift agrees well with the low-wavenumber Raman spectra of LHHM reported by Faria et al. [12]. Such a shift is usually ascribed to the increased bond lengths due to thermal expansion [24,26]. Faria et al. also observed a splitting at 124 cm^{-1} and suggested that the emergence of additional modes were associated with a structural phase transition in LHHM. However, there is no obvious phase transition observed in our experiment. In addition, all of the observed absorption peaks become sharper at lower temperature, owing to the temperature dependent change in the distribution of occupied energy states [27]. These observations suggest that THz spectroscopy is sensitive to the change of temperature.

Table 1
The measured absorption peaks of LHis.

Absorption peak/THz		
This paper	Ref. [17] [a]	Ref. [16]
0.77	0.77	0.70
		1.40
1.73	1.72	1.70
2.09	2.08	2.10
		2.40
2.47	2.50	2.50
2.80	2.83	2.80
2.99		3.00
		3.22
3.37		3.35
		3.48
3.97		

[a] Data in reference are represented in wavenumber, here we convert them to THz frequency, and 1 THz ≈ 33.3333 cm^{-1}.

4.3. Quantum chemical calculation of LHHM

Quantum chemical calculation has been proved to be an effective mean to interpret and understand the experimental THz spectra [28]. The simulation of LHHM based on the previous published crystal cell parameters is proved to be reliable according to the PXRD pattern (Supplementary Materials, Fig. S1). The simulated THz spectra are plotted with the experimental THz spectra of LHHM in Fig. 5. Compared to the experimental peaks, the calculated peaks take a certain degree of shift, which can be attributed to the temperature difference between simulations (at absolute zero) and experiments (at room temperature). Besides, the disparity of crystal formation in actual experiments and theoretical simulations also should be taken into account, since the calculation is based on the perfect crystal structure, while it is difficult to idealize in the actual experimental measurement.

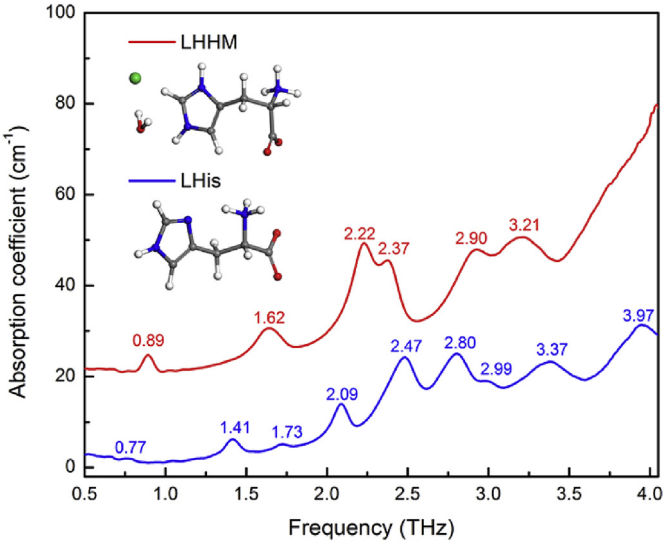

Fig. 2. The THz absorption spectra of LHHM and LHis at 20 °C.

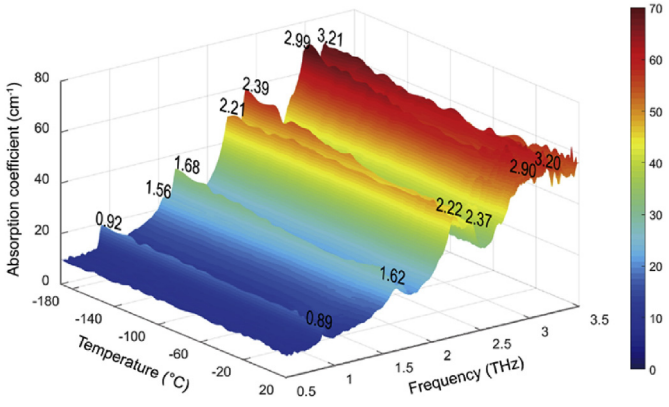

Fig. 3. Evolution of the THz spectra of LHHM from −190 to 20 °C. (The color bar stands for the magnitude of absorption coefficient.). (For interpretation of the references to color in this figure legend, the reader is referred to the Web version of this article.)

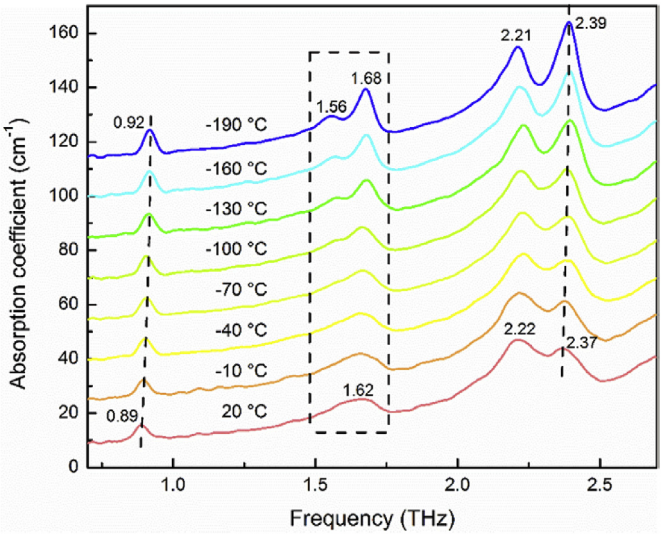

Fig. 4. The temperature effect on the absorption spectra of LHHM.

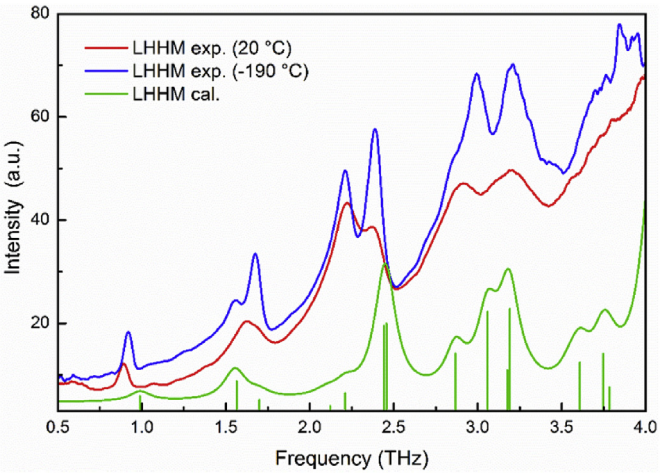

Fig. 5. The experimental and calculated spectra of LHHM.

The typical vibrations in the THz region are described as intermolecular vibrations and molecular flexing [14], which usually involve many atoms even collective vibrations of the whole molecules in the unit cell. Matei et al. [29] summarized that the low-energy vibrational modes of several amino acids below 200 cm^{-1} were related to hydrogen bond interactions. As for LHHM, Faria et al. [12] associated all the bands appearing under 200 cm^{-1} with external lattice modes of the crystal. To better understand the low-frequency vibrations of LHHM, the intra- and intermolecular hydrogen bonds are depicted in Fig. 6 (a). It is shown that each molecule is linked by a network of eight hydrogen bonds to neighboring molecules of water, chlorine, and histidine [30]. The hydrogen-bond network of LHHM lattices is exhibited in Fig. 6 (b). It is believed that the stability of the structure of amino acid is determined by the distribution and the quantity of hydrogen bonds in the unit cell [31]. For a clear identification of vibrational modes, three typical vibrational modes of LHHM are demonstrated in Fig. 7. The peak at 1.62 THz at 20 °C splits into two peaks (1.56 and 1.68 THz) at −190 °C, which can be attributed to the calculated mode from 1.56 to 1.70 THz, due to the translation of −COO$^-$ group with imidazole ring and water molecule in different direction. The measured feature at 2.22 THz is relative to the simulated mode at

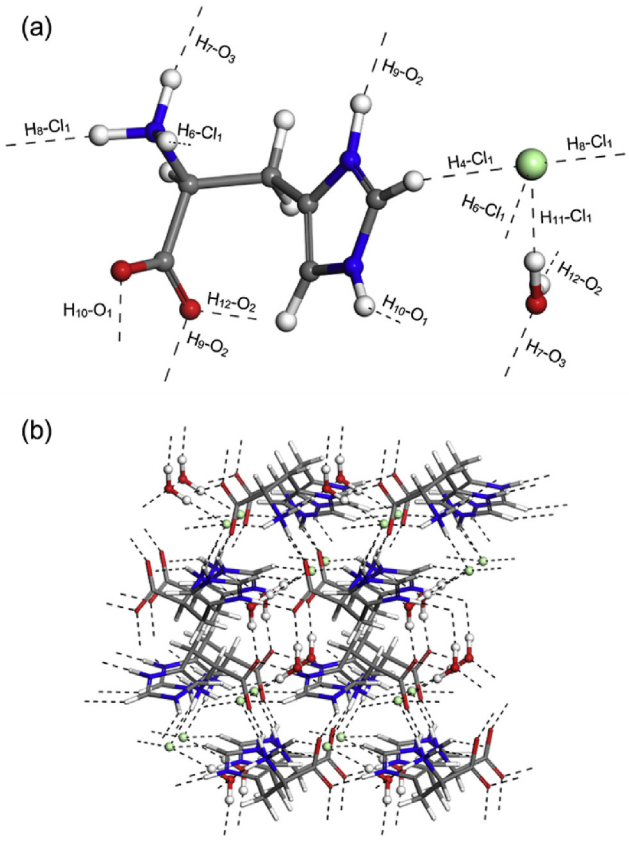

Fig. 6. (a) The hydrogen bonds (the black dash lines) of one LHHM molecule in lattice; (b) the hydrogen-bond network of LHHM lattices.

2.21 THz, which originates from rotational vibration of $-NH_3^+$ group with −COO$^-$ group and translation of imidazole ring and water molecule. The experimental peak at 3.20 THz corresponds to the vibrational mode calculated at 3.19 THz, attributing to the stretching vibration of the hydrogen bond besides the torsion of LHis molecule and the translation of Cl$^-$ and water in the same direction. The detailed descriptions of the calculated vibrational modes of LHHM were presented in Table 2.

5. Conclusion

In this work, THz spectroscopy was employed to investigate the powder crystal L-histidine hydrochloride derivative LHHM. The low-frequency absorption spectrum of LHHM was observed over 0.5–4.0 THz and then compared with the THz spectrum of amino acid LHis. The distinctive spectra of LHHM and LHis indicate that the characteristic THz fingerprints can be used in detection and identification applications. The temperature dependence of the vibrational modes of LHHM was monitored. It was found that as the temperature decreased, the observed absorption bands become sharper and shift towards higher frequencies, and the peak at 1.62 THz split into two at low temperature. The observation manifests that THz spectroscopy is sensitive to the change of temperature. Furthermore, the frequency calculation and individual vibrational modes assignment of LHHM were performed by adopting DFT method. The results show that THz absorption spectra mainly reflect the collective vibrational motions of the whole molecule, including imidazole ring, zwitterionic backbone, Cl$^-$ and water molecule. Intermolecular hydrogen bonds were also found to have the contribution to the low-frequency vibrations.

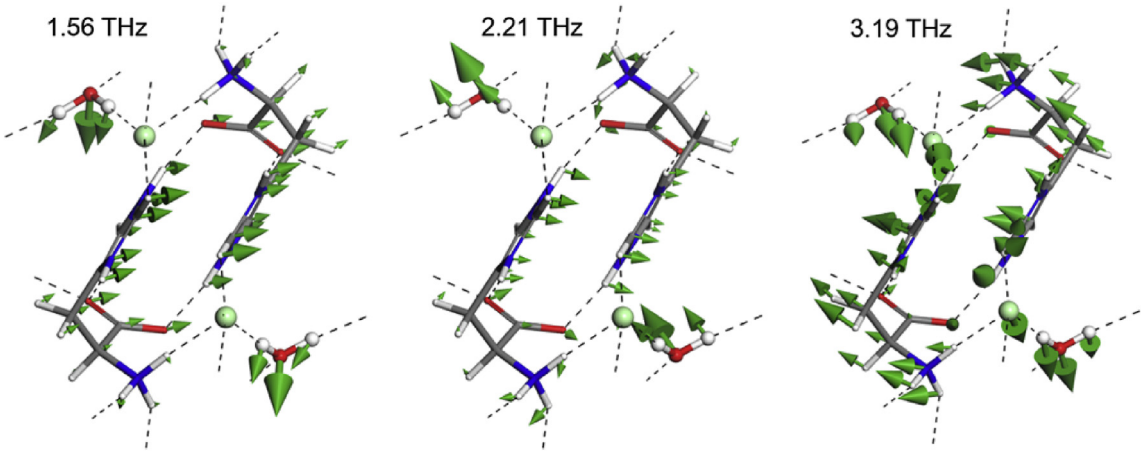

Fig. 7. The calculated vibrational modes of LHHM at 1.56, 2.21, and 3.19 THz, respectively.

Table 2
The spectral features and the corresponding vibrational modes of LHHM.

Exp./THz		Cal./THz	Ref. [12] [a]/THz	Vibrational mode assignment
20 °C	−190 °C			
0.89	0.92	0.99		collective translation of LHis, H_2O and Cl^-
1.62	1.56	1.56	1.56	translation of $-COO^-$ group with imidazole ring and H_2O in different direction
	1.68	1.70		translation of H_2O
			1.95	
2.22	2.21	2.21	2.28	rotation of $-NH_3^+$ group with $-COO^-$ group and translation of imidazole ring and H_2O
2.37	2.39	2.44		translation of imidazole ring and Cl^-; rotation of zwitterionic backbone
		2.45		translation of Cl^- and H_2O in different direction
2.90	2.99	2.87	2.94	torsion of LHis and translation of H_2O
		3.06		rotation of LHis and translation of H_2O and Cl^- with HB vibration[a]
3.20	3.21	3.19	3.24	torsion of LHis and translation of Cl^- and H_2O with HB vibration[a]

[a] Raman spectroscopy data in reference are converted to THz frequency, 1 THz ≈ 33.3333 cm^{-1}; "HB" stands for hydrogen bond.

Acknowledgements

This work was supported by the Main Direction Program of Knowledge Innovation and Open Project Program of Key Laboratory of Interfacial Physics and Technology, Chinese Academy of Sciences, the National Science Foundation [No. 11604359].

Appendix A. Supplementary data

Supplementary data related to this article can be found at https://doi.org/10.1016/j.molstruc.2017.12.088.

References

[1] G.N. Chen, X.P. Wu, J.P. Duan, et al., A study on electrochemistry of histidine and its metabolites based on the diazo coupling reaction, Talanta 49 (1999) 319–330. https://dx.doi.org/10.1016/S0039-9140(98)00379-8.
[2] S. Kumar, A.K. Rai, S.B. Rai, et al., Infrared and Raman spectra of histidine: an ab initio DFT calculations of histidine molecule and its different protonated forms, Indian J. Phys. 84 (2010) 563–573. https://doi.org/10.1007/s12648-010-0039-6.
[3] M.O. Iwunze, The characterization of the fluorescence of L-histidine in simulated body fluid, J. Photochem. Photobiol. A 186 (2007) 283–289. https://doi.org/10.1016/j.jphotochem.2006.05.034.
[4] C. Bermúdez, S. Mata, C. Cabezas, et al., Tautomerism in neutral histidine, Angew. Chem. Int. Ed. 53 (2014) 11015–11018. https://dx.doi.org/10.1002/anie.201405347.
[5] H.O. Marcy, L.A. DeLoach, J.H. Liao, et al., L-histidine tetrafluoroborate: a solution-grown semiorganic crystal for nonlinear frequency conversion, Optic Lett. 20 (1995) 252–254. https://dx.doi.org/10.1364/OL.20.000252.
[6] R. Ittyachan, P. Sagayaraj, Growth and characterization of a new promising NLO L-histidine bromide crystal, J. Cryst. Growth 249 (2003) 557–560. https://doi.org/10.1016/S0022-0248(02)02116-4.
[7] A.B. Ahmed, H. Feki, Y. Abid, et al., Structural, vibrational and theoretical studies of L-histidine bromide, J. Mol. Struct. 888 (2008) 180–186. https://doi.org/10.1016/j.molstruc.2007.11.056.
[8] P. Anandan, M. Arivanandhan, Y. Hayakawa, et al., Investigations on the growth aspects and characterization of semiorganic nonlinear optical single crystals of L-histidine and its hydrochloride derivative, Spectrochim. Acta A 121 (2014) 508–513. https://doi.org/10.1016/j.saa.2013.11.021.
[9] M. Baranska, M. Roman, K. Majzner, General overview on vibrational spectroscopy applied in biology and medicine, in: M. Baranska (Ed.), Optical Spectroscopy and Computational Methods in Biology and Medicine, Springer, Netherlands, 2014, pp. 3–14. https://doi.org/10.1007/978-94-007-7832-0_1.
[10] P. Anandan, R. Jayavel, T. Saravanan, et al., Crystal growth and characterization of L-histidine hydrochloride monohydrate semiorganic nonlinear optical single crystals, Opt. Mater. 34 (2012) 1225–1230. https://doi.org/10.1016/j.optmat.2012.01.042.
[11] A. Ben Ahmed, H. Feki, Y. Abid, et al., Crystal studies, vibrational spectra and non-linear optical properties of L-histidine chloride monohydrate, Spectrochim Acta A 75 (2010) 293–298. https://dx.doi.org/10.1016/j.saa.2009.10.026.
[12] J.L.B. Faria, F.M. Almeida, O. Pilla, et al., Raman spectra of L-histidine hydrochloride monohydrate crystal, J. Raman Spectrosc. 35 (2004) 242–248. https://dx.doi.org/10.1002/jrs.1142.
[13] M.D. King, T.M. Korter, Effect of waters of crystallization on terahertz spectra: anhydrous oxalic acid and its dihydrate, J. Phys. Chem. A 114 (2010) 7127–7138. https://dx.doi.org/10.1021/jp101935n.
[14] A.C. Jørgensen, C.J. Strachan, K.H. Pöllänen, et al., An insight into water of crystallization during processing using vibrational spectroscopy, J. Pharm. Sci. 98 (2009) 3903–3932. https://dx.doi.org/10.1002/jps.21735.
[15] M.D. King, W.D. Buchanan, T.M. Korter, Understanding the terahertz spectra of crystalline pharmaceuticals: terahertz spectroscopy and solid-state density functional theory study of (S)-(+)-ibuprofen and (RS)-ibuprofen, J. Pharm. Sci. 100 (2011) 1116–1129. https://dx.doi.org/10.1002/jps.22339.
[16] A.B. True, K. Schroeck, T.A. French, et al., Terahertz spectroscopy of histidine enantiomers and polymorphs, J. Infrared Millim. Terahertz Waves 32 (2011) 691–698. https://dx.doi.org/10.1007/s10762-010-9645-9.
[17] R. Rungsawang, Y. Ueno, I. Tomita, et al., Angle-dependent terahertz time-domain spectroscopy of amino acid single crystals, J. Phys. Chem. B 110 (2006) 21259–21263. https://dx.doi.org/10.1021/jp060492n.
[18] Y. Shi, L. Wang, Collective vibrational spectra of α- and γ-glycine studied by

terahertz and Raman spectroscopy, J. Phys. D Appl. Phys. 38 (2005) 3741. https://doi.org/10.1088/0022-3727/38/19/024.
[19] F. D'Angelo, Z. Mics, M. Bonn, et al., Ultra-broadband THz time-domain spectroscopy of common polymers using THz air photonics, Optic Express 22 (2014) 12475–12485. https://dx.doi.org/10.1364/OE.22.012475.
[20] H. Fuess, D. Hohlwein, S.A. Mason, Neutron diffraction study of L-histidine hydrochloride monohydrate, Acta Crystallogr. B 33 (1977) 654–659. https://dx.doi.org/10.1107/S0567740877004415.
[21] M.S. Lehmann, T.F. Koetzle, W.C. Hamilton, Precision neutron diffraction structure determination of protein and nucleic acid components. IV. The crystal and molecular structure of the amino acid L-histidine, Int. J. Pept. Protein Res. 4 (1972) 229–239. https://dx.doi.org/10.1111/j.1399-3011.1972.tb03424.x.
[22] S.J. Clark, M.D. Segall, C.J. Pickard, et al., First principles methods using CASTEP, Z. Kristallogr. 220 (2005) 567–570. https://dx.doi.org/10.1524/zkri.220.5.567.65075.
[23] J.P. Perdew, K. Burke, M. Ernzerhof, Generalized gradient approximation made simple, Phys. Rev. Lett. 77 (1996) 3865–3868. https://dx.doi.org/10.1103/PhysRevLett.77.3865.
[24] M. Takahashi, Terahertz vibrations and hydrogen-bonded networks in crystals, Crystals 4 (2014) 74–103. https://dx.doi.org/10.3390/cryst4020074.
[25] F. Pflüger, B. Hernández, M. Ghomi, Vibrational analysis of amino acids and short peptides in hydrated media. VII. Energy landscapes, energetic and geometrical features of L-histidine with protonated and neutral side chains, J. Phys. Chem. B 114 (2010) 9072–9083. https://dx.doi.org/10.1021/jp103348y.
[26] L.M. Lepodise, J. Horvat, R.A. Lewis, Terahertz spectroscopy of 2,4-dinitrotoluene over a wide temperature range (7–245 K), J. Phys. Chem. A 119 (2015) 263–270. https://dx.doi.org/10.1021/jp5052134.
[27] Y.C. Shen, P.C. Upadhya, E.H. Linfield, et al., Temperature-dependent low-frequency vibrational spectra of purine and adenine, Appl. Phys. Lett. 82 (2003) 2350–2352. https://dx.doi.org/10.1063/1.1565680.
[28] D.F. Plusquellic, K. Siegrist, E.J. Heilweil, et al., Applications of terahertz spectroscopy in biosystems, ChemPhysChem 8 (2007) 2412–2431. https://dx.doi.org/10.1002/cphc.200700332.
[29] A. Matei, N. Drichko, B. Gompf, et al., Far-infrared spectra of amino acids, Chem. Phys. 316 (2005) 61–71. https://dx.doi.org/10.1016/j.chemphys.2005.04.033.
[30] E. Westhof, W. Flossmann, A. Müller, E.S.R. and INDO study of radicals produced in irradiated single crystals of histidine hydrochloride monohydrate at low temperature, Mol. Phys. 28 (1974) 151–160. https://dx.doi.org/10.1080/00268977400101581.
[31] G.P. De Sousa, P.T.C. Freire, J. Mendes Filho, et al., Low-temperature raman spectra of L-histidine crystals, Braz. J. Phys. 43 (2013) 137–144. https://dx.doi.org/10.1007/s13538-013-0132-3.